Chapter 13
Quantification of Vibrational Power Dissipation in a Coupled Panel System Using Experimental Modal Analysis

Karsten Hilgarth, Yeongeun Ki, Daniel Litowitz, Eric Williamson, Karthik Boddapati, Hongcheng Tao, Charlotte Moss, Greg Shaver, John T. Evans, Andres F. Arrieta, and James M. Gibert

Abstract To quantify the vibrational energy available in composite panels used in the construction of semi-truck trailers, this work investigates the power dissipated through internal damping as these panels undergo dynamic loading during road travel. Modal impact testing of a single 1.24 m x 2.49 m panel was conducted to extract the structure's natural frequencies, mode shapes, and damping ratios. Using this modal model, operational acceleration data collected during road testing were projected into modal coordinates and integrated to obtain modal velocities. These velocities, combined with the previously identified modal parameters, were used to estimate the instantaneous power dissipated in the dominant modes. The resulting average power dissipation reflects the rate at which vibrational energy is lost through internal damping and serves as a minimal upper bound for the mechanical energy that could be harvested using passive devices. Results across 19 road segments show that the average dissipated power ranges from ~ 0.5–20 W, with peak values exceeding 6 kW during transient events. These results support the future development of piezoelectric or triboelectric energy harvesters integrated into trailer panels to help reduce the alternator load in heavy vehicles.

Keywords Experimental modal analysis · Operational data · Vibrations · Power dissipation · Energy scavenging

Introduction

Commercial vehicle manufacturers are investigating methods to reclaim energy that is typically wasted during operation to enhance efficiency. A viable method involves extracting vibrational energy from trailer sidewall panels, which are frequently stimulated by uneven road surfaces, powertrain vibrations, and wind during transit. As a result these lightweight composite panels waste energy through continuous vibrations, and partial recovery of this energy could decrease alternator demand, enhancing fuel efficiency and reducing emissions [1]. Nevertheless, a significant knowledge gap exists due to the absence of quantification of the panel's vibrational energy. Quantifying the available vibrational energy and comprehending its dissipation within panel structures is crucial for the design and integration of energy harvesters. This effort aims described here outlines the development evaluation of a framework for quantifying the vibrational energy wasted in trailer panels through experimental modal analysis and in-situ road testing.

This work provides a framework for assessing the energy available for different transduction methodologies ranging from electromagnetic to piezoelectric [2, 3] to triboelectric harvesting [4]. The results from this study provide an estimate of dissipated energy, advancing both the understanding of trailer panel dynamics and the development of technologies aimed at increasing the energy efficiency of heavy vehicles.

Karsten Hilgarth · Yeongeun Ki · Daniel Litowitz · Eric Williamson · Karthik Boddapati · Hongcheng Tao · Charlotte Moss · Greg Shaver · John T. Evans · Andres F. Arrieta · James M. Gibert
Ray W. Herrick Laboratories, School of Mechanical Engineering, Purdue University, West Lafayette, IN 47096
e-mail: khilgart@purdue.edu; yki@purdue.edu; dlitowit@purdue.edu; will1904@purdue.edu; kboddapa@purdue.edu; taoh@purdue.edu; moss66@purdue.edu; gshaver@purdue.edu; jevansiv@purdue.edu; aarrieta@purdue.edu; jgibert@purdue.edu

John T. Evans
Department of Agriculture and Biological Engineering, Purdue University, West Lafayette, IN 47096
e-mail: jevansiv@purdue.edu

Kristin B. Zimmerman, PhD (eds.), *Topics in Modal Analysis & Parameter Identification in Structural Dynamics, 2026, Vol. 8*,
Conference Proceedings of the Society for Experimental Mechanics Series, https://doi.org/10.1007/978-8-743-81447-4_13

The remainder of this paper is organized as follows: the methodology integrating experimental modal analysis with operational road testing is described first, followed by details of the experimental setup and data collection procedures. The subsequent section presents the framework for estimating vibrational power dissipation in modal coordinates, with results from multiple road segments provided for comparison. A discussion of the implications for energy harvesting applications is then given, and the paper concludes with key findings and directions for future research.

Methodology

This study's methodology combines experimental modal analysis with operational observations to assess vibrational energy dissipation in trailer panels. First, modal properties, i.e., natural frequencies, damping ratios, and mode shapes, are identified from controlled impact testing. These parameters establish a reduced-order modal model of the panel. Next, *in-situ* acceleration data are collected under real driving conditions and projected into modal coordinates, enabling the estimation of modal velocities. Finally, the damping related power dissipation is computed in the modal domain, taking advantage of the invariance of power under the transformation between physical and modal coordinates. This combined framework provides a consistent means of linking laboratory based modal characterization with field measurements, thereby allowing reliable estimates of the energy available for harvesting in operational environments.

Experimental Modal Analysis (EMA)

In order to determine the energy dissipated by the panels, the modal properties of the panel were first obtained experimentally. Figure 1 (a) shows the experimental setup used for the modal analysis. The modal analysis is performed on the first full panel from the rear of the trailer. The panel has a width, height, and thickness of approximately 1.24 m x 2.49 m x 0.05 m ($\approx$ 48.8 in × 98.0 in × 2.0 in), and a weight of 38 kg ($\approx$ 83.8 lb). In order to facilitate non-contact measurement, reflective tape is placed on the panel at each of the 25 defined measurement points, as shown in Figure 1 (b). The vibration at each point is measured using a PSV 400-Laser Doppler Vibrometer (LDV), which provides velocity measurements without mass-loading the lightweight panel structure. The system is excited by an instrumented modal hammer (PCB Model 086D20) to provide a broadband, measurable force input, $F(t)$. The hammer is used to excite the panel from inside the trailer at location 13.

For each impact, the LDV records the velocity response of the sample as a function of time, $v(t)$. This time-domain data is then processed to determine the system's frequency response characteristics. Fast Fourier Transform (FFT) is applied to both the input force signal and the output velocity signal to transform them into the frequency domain, yielding the spectra $F(f)$ and $V(f)$.

From these spectra, the Frequency Response Function (FRF) is calculated. The H_1 estimator is typically used for this analysis, as it is formulated to minimize the effect of noise on the output (response) measurement, which is common in experimental setups. The H_1 FRF is calculated as the ratio of the cross-spectrum (G_{fv}) to the auto-spectrum of the input (G_{ff}):

$$H_1(f) = \frac{G_{fv}(f)}{G_{ff}(f)} = \frac{V(f)F^*(f)}{F(f)F^*(f)}, \tag{1}$$

where $F^*(f)$ is the complex conjugate of the force spectrum. Figure 2 shows the plots of Equation 1 for all 25 measurement points and the single excitation point. The quality and linearity of the measurement at each frequency are assessed using the coherence function, $\gamma^2(f)$. A coherence value close to 1.0 indicates a strong linear relationship between the input force and the output response, signifying the structure has sufficient energy to respond at that frequency. Conversely, drops in coherence can indicate noise contamination or nonlinear behavior. In this study $\gamma^2(f) > 0.9$ from 3 to 179 Hz for most points.

Once a set of FRFs is collected for all measurement points on the panel, modal parameter estimation algorithms are employed. These algorithms fit a theoretical modal model to the experimental FRF data to extract the key dynamic properties of the panel as installed: its natural frequencies (ω_n), modal damping ratios (ζ_n), and the corresponding mode shapes ($\vec{\psi}_n$).

Using the FRFs collected for all measurement points on the panel, modal parameters are extracted [5]. Since modal frequency and damping are global properties of the structure, a Global Curve Fitting approach is employed, as described by Richardson and Formenti [6]. This method leverages the entire set of FRF measurements simultaneously to yield a single, consistent set of modal parameters that is more robust than fitting each measurement individually.

The Rational Fraction Polynomial (RFP) method [6] is used to extract modal frequencies and damping ratios from the experimentally obtained frequency response functions. The method fits a ratio of two polynomials to the experimental FRF

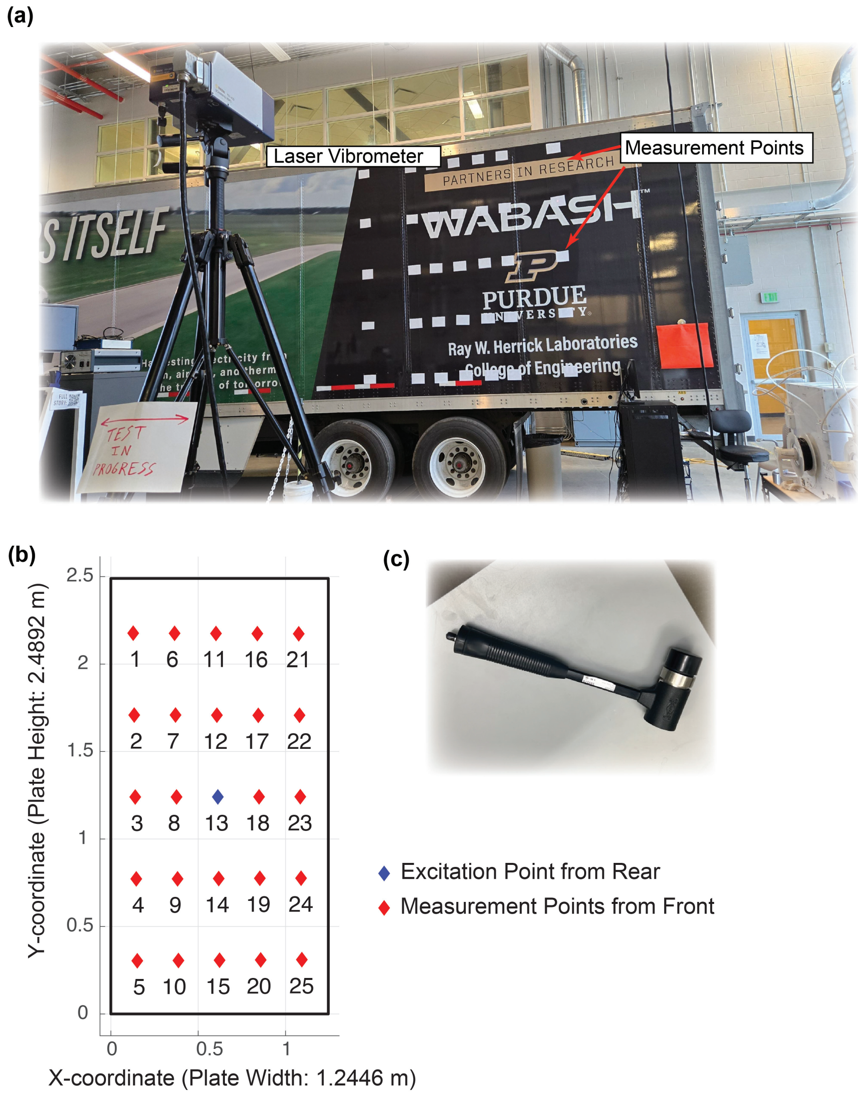

Fig. 1 Experimental setup to measure modeshapes of an individual panel: (a) photo of test setup (b) schematic of sensor locations, and (c) modal impact hammer (PCB Modal 086D20)

data. The roots of the denominator polynomial, known as the system poles, are identified. Each complex-conjugate pair of poles corresponds to a single mode of vibration. For each mode n, the pole p_n is given by:

$$p_n = -\sigma_n + j\omega_{dn}, \tag{2}$$

where σ_n is the damping factor and ω_{dn} is the damped natural frequency. The undamped natural frequency, ω_n, and the modal damping ratio, ζ_n, are then calculated from these pole values:

$$\omega_n = \sqrt{\sigma_n^2 + \omega_{dn}^2} \quad \text{and} \quad \zeta_n = \frac{\sigma_n}{\omega_n}. \tag{3}$$

This global estimation process yields a single, consistent value for the natural frequency and damping ratio for each mode.

The unscaled mode shape amplitudes at the discrete measurement points are estimated by taking the imaginary component of the FRF at each respective modal frequency. Biharmonic spline interpolation is then used to visualize the continuous mode shape across the panel surface, as shown in Figure 3. The first mode at 4.0 Hz is a simple bending mode along the panel's long axis. The second mode at 12.63 Hz exhibits a torsional or twisting motion. The third (24.6 Hz) and fourth (44.88 Hz) modes show higher-order bending and combined bending-torsion shapes, respectively. The fifth mode at 130 Hz is a

Table 1 Modal Frequencies and Damping Ratios of Wall Panel

Mode No. (n)	**Modal Frequencies** (ω_n)	**Damping Ratios** (ζ_n)
1	4.00 Hz	0.033
2	12.63 Hz	0.014
3	24.60 Hz	0.008
4	44.88 Hz	0.006
5	130.00 Hz	0.006

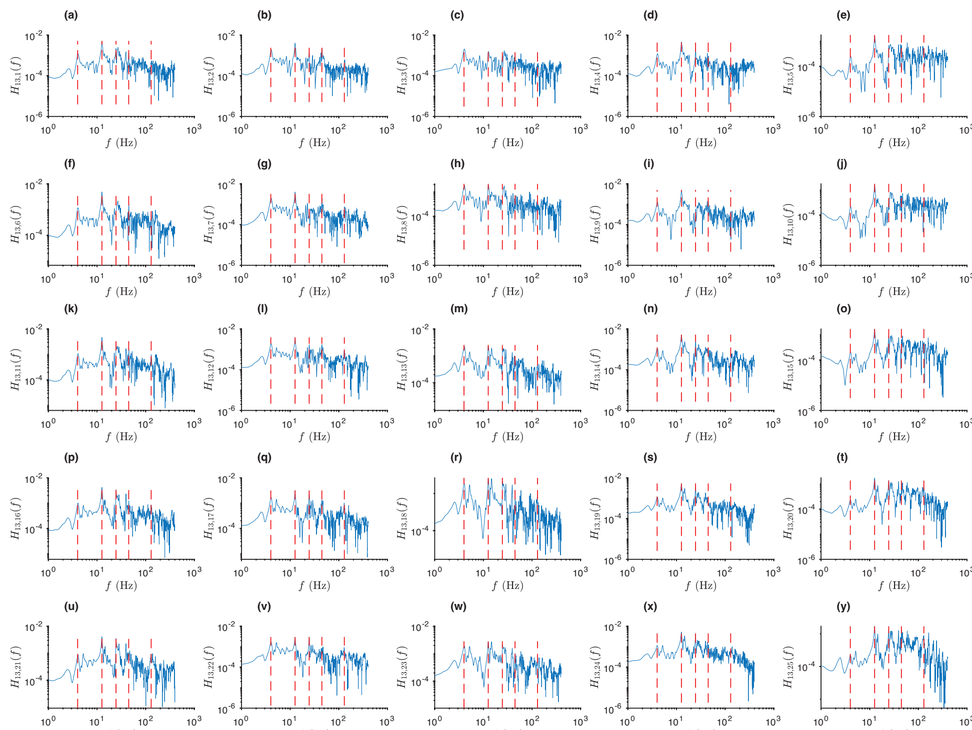

Fig. 2 Frequency Response Function magnitudes for all 25 measurement points relative to the excitation at point 13. The consistency of peak locations across all plots confirms the presence of global structural modes. Red dashed lines indicate the first five modal frequencies identified and used for subsequent power dissipation analysis. The consistency of peaks across FRFs enables a robust global fit

more complex, higher-order plate mode. These five modes were mass normalized and form the basis of the modal model used for subsequent analysis.

Operational Analysis During Road Transport

Figure 4 a) shows the experimental setup used for the operational analysis. The analysis was again conducted on the first full panel from the rear. To capture the panel's response under real-world conditions, five accelerometers (PCB 352C04 and PCB 352A60) are placed on the inside of the panel at key locations. The accelerometers are connected to a Keyence NR-X data logger with an Accelerometer (NR-CA04) module, which records their outputs.

The purpose of this test is to measure the panel's absolute acceleration time histories, $a_k(t)$, while the semi-trailer is driven on public roads. This provides a set of response data that results from the true broadband random excitation input from the road surface, suspension dynamics, and aerodynamic forces. This operational acceleration data serves as the input to the modal model, allowing the projection of the measured physical response onto the previously identified modal coordinates.

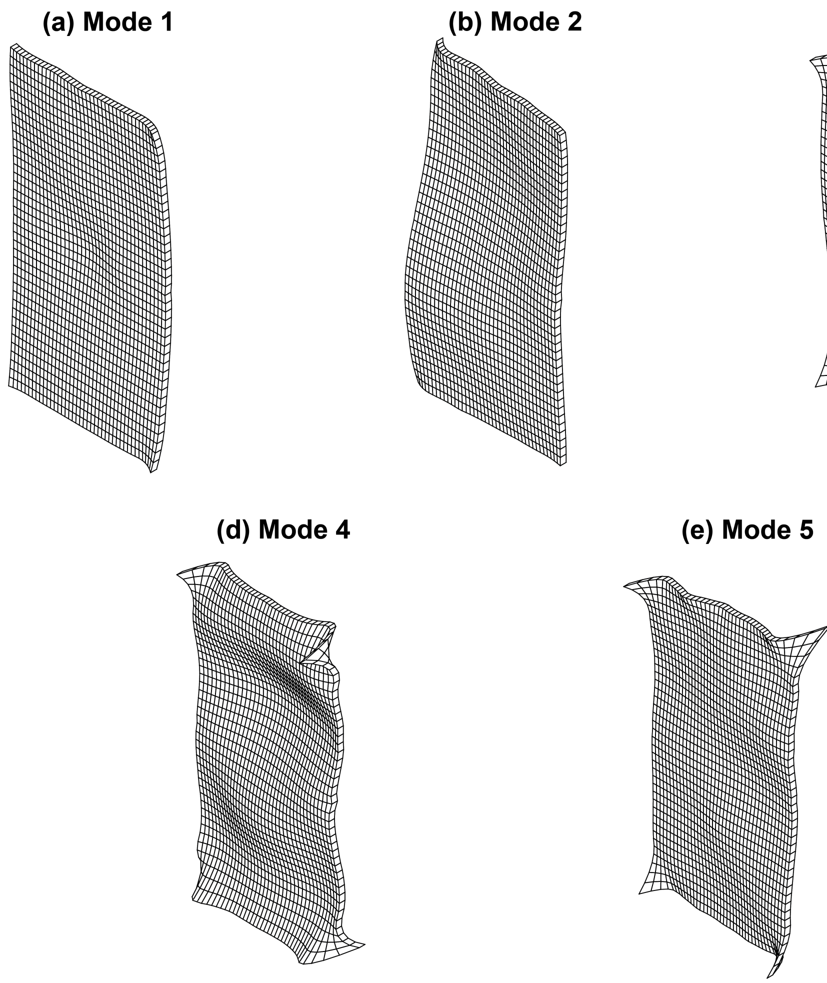

Fig. 3 Five modeshapes of rear panel used in this study: (a) first mode is 4 Hz, (b) second mode is 12.63 Hz, (c) third mode is 24.63 Hz, (d) fourth mode is 44.88 Hz and (e) fifth mode is 130 Hz

The route taken by the trailer in West Lafayette, Indiana is shown in Figure 5. The route consisted of 19 different road segments, named in Figure 5. Figure 6 plots the Power Spectral Density (PSD) for an accelerometer (S1) across the 19 different road segments revealing several consistent patterns in the vibrational environment experienced by the trailer panels. Power spectral density (PSD) estimates were obtained using Welch's method. Unless otherwise noted, the MATLAB pwelch function was applied with parameters: a Hamming window of 256 samples, 50% overlap (128 samples), and a 768-point FFT. With the sampling frequency of $f_s = 1000$ Hz, this configuration provides a frequency resolution of approximately 3.9 Hz based on 256 samples. PSD results are reported in units of power per Hz, using a one-sided spectrum since all signals were real-valued. Across nearly all roads, the dominant spectral energy is concentrated in the low frequency range below 20 Hz, which is typical of road induced base excitation where long-wavelength surface irregularities excite suspension and structural modes. While all roads show broadband excitation extending up to 50–60 Hz, certain segments, such as SR43, SR26, and I65, exhibit notably higher PSD amplitudes, indicating more aggressive vibrational input likely due to surface roughness, speed, or joint transitions. In contrast, roads like US421 show relatively lower energy levels, suggesting smoother or better-maintained pavement. Importantly, the PSDs do not exhibit sharp resonant peaks, implying that structural modes are either well-damped or not strongly excited during typical driving conditions. This behavior suggests that energy harvesting strategies should focus on broadband response within the 2–20 Hz range, rather than tuning to narrowband resonances. These observations also support the classification of roads by excitation severity, providing a basis for fatigue, damage, or energy harvesting analysis under representative operational loading conditions.

To assess whether the acceleration signals could be treated as broadband random processes suitable for power spectral analysis, statistical descriptors were computed in 30-s windows across the full I-65 dataset. For the acceleration signal $a(t)$

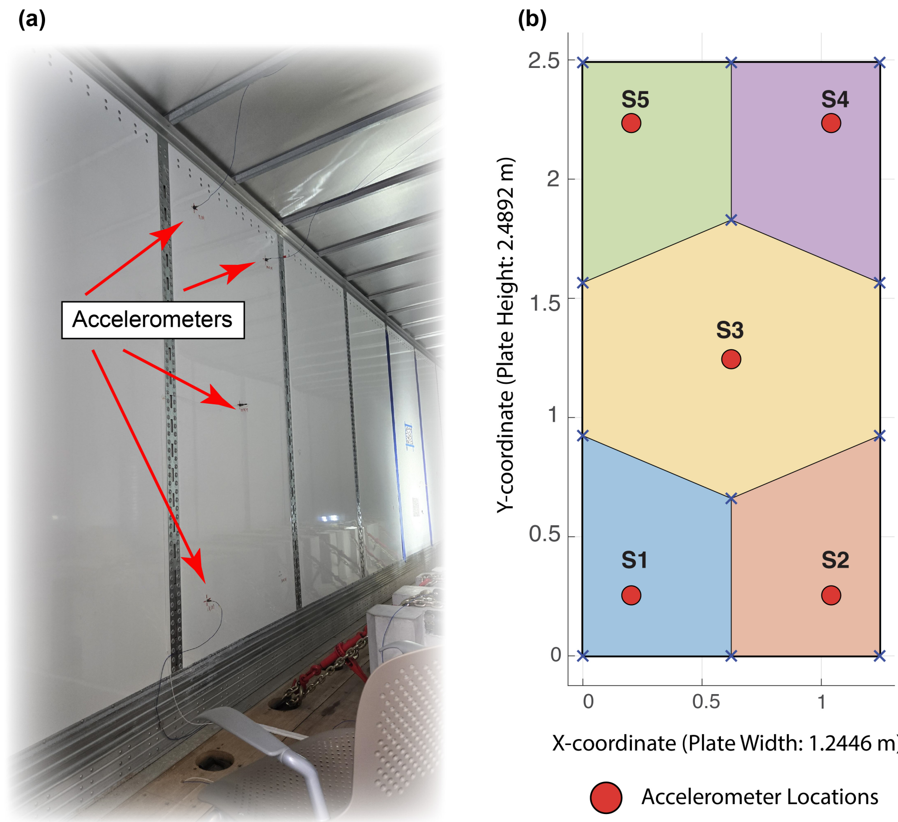

Fig. 4 Experimental setup to perform operational analysis: (a) location of accelerometer, and (b) accelerometer locations and Voronoi tesselation of mass for modal analysis

sampled at N points, the time-domain statistics were computed as:

$$\mathrm{RMS} = \sqrt{\frac{1}{N}\sum_{i=1}^{N} a_i^2}, \quad \text{Crest Factor} = \frac{\max|a_i|}{\mathrm{RMS}}, \quad \text{and} \quad \text{Kurtosis} = \frac{\frac{1}{N}\sum_{i=1}^{N}(a_i-\bar{a})^4}{\left(\frac{1}{N}\sum_{i=1}^{N}(a_i-\bar{a})^2\right)^2}, \tag{4}$$

where $\bar{a}$ is the sample mean.

The results indicate non-stationary but predominantly random-like behavior. RMS values varied from 0.18 to 0.80 m/s^2, with occasional peaks as high as 7.9 m/s^2. Crest factors typically ranged between 4 and 6, though extreme values above 12 were observed, suggesting intermittent impulsive events. Kurtosis values were generally near Gaussian expectations (3–6) but reached as high as 19–24 in isolated windows, further confirming the presence of rare, heavy-tailed transients.

Table 2 Summary statistics for I-65 acceleration data (30-s windows)

Metric	Typical Range	Extreme Values	Interpretation
RMS (m/s^2)	0.18–0.80	–	Varies with road roughness
Peak (m/s^2)	1–3	7.9	Rare large impulses
Crest Factor	4–6	12.9	Broadband with transients
Kurtosis	3–6	19–24	Heavy-tailed distribution

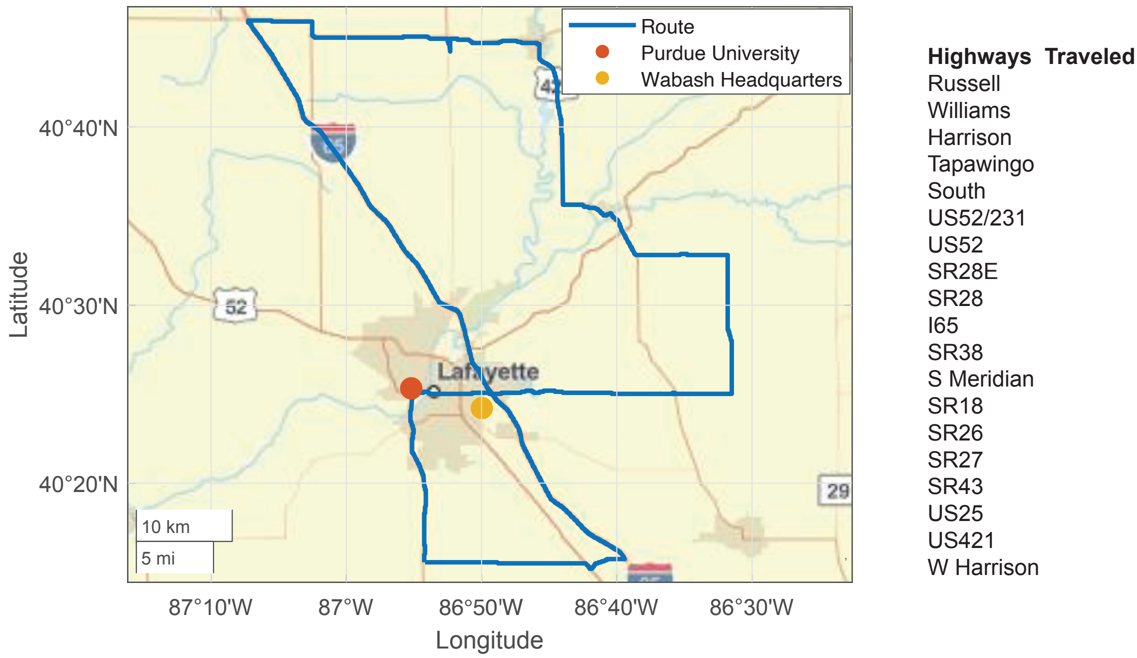

Fig. 5 Route driven in West Lafayette, Indiana by the semi-truck trailer during operational testing to collect panel acceleration data. The loop incorporated 19 distinct road segments, ranging from local streets to interstate highways, providing a diverse set of excitation environments. These segments form the basis for the comparative power and energy dissipation analysis presented in Table 3

Methodology for Energy Dissipation

The following analysis focuses on a single instrumented panel within a larger assembly of 12 coupled panels. The boundary conditions are addressed implicitly; by measuring the modal parameters *in situ*, the stiffening and mass-loading effects of the adjacent panels are inherently captured in the measured mode shapes ($\vec{\psi}_n$) and natural frequencies (ω_n). The calculated power, P_{measured}, represents the energy converted to heat (dissipated) within this single panel due to its internal damping. This calculation is based on the panel's net response, which is the result of all energy inputs from the frame and adjacent panels. It is important to note that this dissipated power is only one of two primary energy pathways for the panel. The second pathway is the net power transmitted across its boundaries to its neighbors, $P_{\text{transmitted}}$. While this analysis does not directly calculate $P_{\text{transmitted}}$, it uses this physical understanding to establish justifiable lower and upper bounds for the energy dissipation of the entire 12-panel system that composes one wall.

Time Domain Modal Velocity Approach

The dissipated vibrational power of the panel is estimated by transforming measured accelerations into modal coordinates and computing the associated damping losses. The procedure consists of four main steps: (i) identification of modal parameters, (ii) estimation of effective mass distribution, (iii) transformation of physical accelerations into modal accelerations and velocities, and (iv) computation of instantaneous and average power. This analsyis is conducted in the time domain since accelerometer signals exhibit quasi-stationary behavior with intermittent transients, as indicated by windowed statistics in Table 2, i.e., RMS variation across windows, crest factors frequently exceeding 6, and occasional high-kurtosis windows). Welch PSD estimates assume in a wide-sense stationarity thus a purely spectral approach can dilute the contribution of short-duration, high-amplitude events. In contrast, our time-domain formulation computes instantaneous modal power and cumulative power and retains the effects of transients. The derivation of the method can be found in the Appendix.

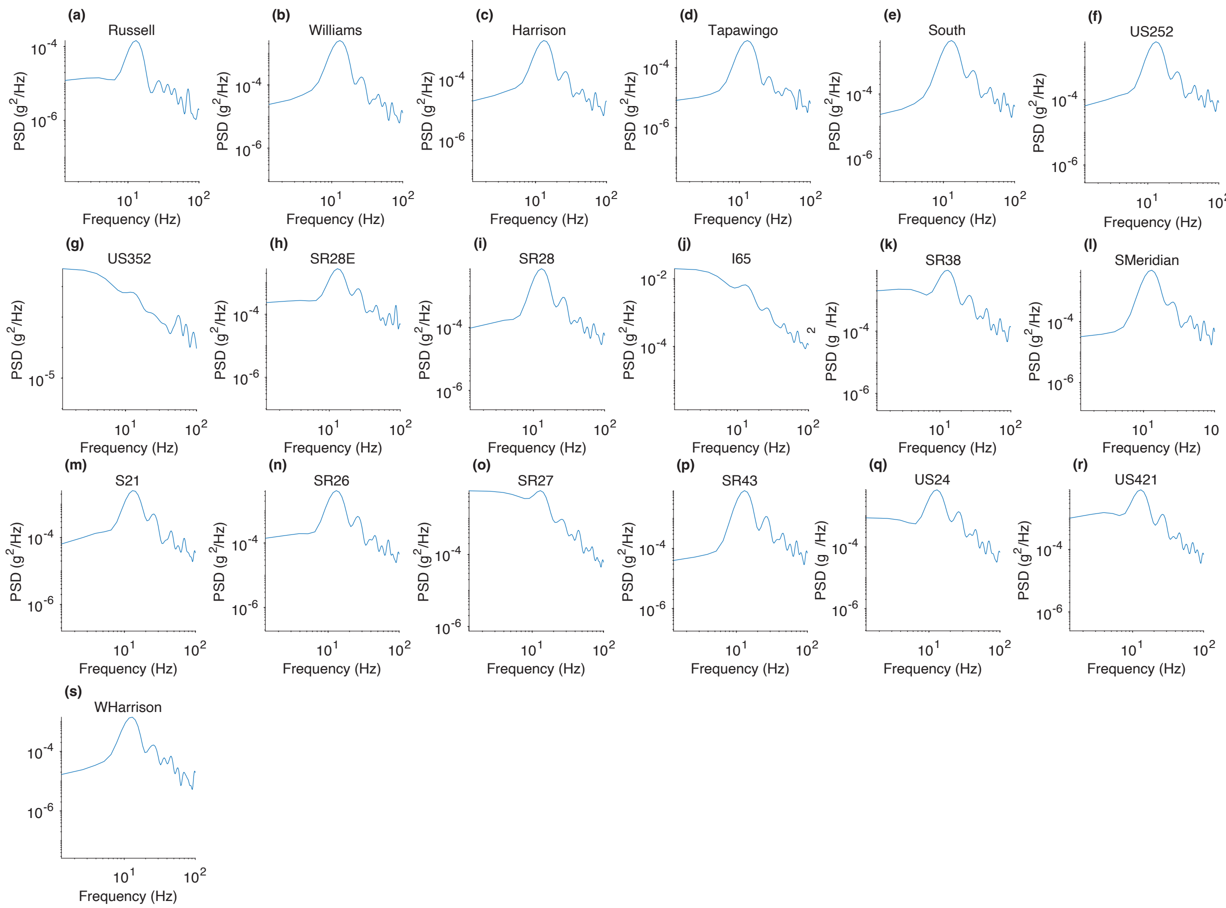

Fig. 6 Power spectral density (PSD) of trailer panel acceleration measured at sensor S1 across 19 road segments. Dominant vibrational content is concentrated below 20 Hz, with broadband excitation extending up to 50–60 Hz. PSDs were estimated using Welch's method (256-sample Hamming window, 50% overlap, 768-point FFT, f_s = 1000 Hz), yielding a frequency resolution of 3.9 Hz. Variations in the number of spectral points across curves reflect differences in road segment duration, as shorter segments contain fewer data samples

Modal Parameter Identification

The experimental modal analysis provided the natural frequencies ω_n, mass-normalized mode shapes $\vec{\psi}_n$, and damping ratios ζ_n for each mode $n = 1, \ldots, N_m$ where N_m is the number of modes retained, i.e, $N_m = 5$ in this study. Because the mode shapes were mass-normalized, the modal mass is unity ($m_n = 1$), and the modal damping coefficient simplifies to

$$c_n = 2\zeta_n\omega_n. \tag{5}$$

Lumped Mass Matrix via Voronoi Tessellation

To account for the spatial distribution of the panel's mass, the physical mass matrix $\mathbf{M}$ is approximated as diagonal with entries M_k representing the effective mass at each measurement location. These lumped values are obtained by partitioning the panel area into Voronoi cells based on sensor positions, clipping the cells to the panel boundary, and scaling by the areal mass density $\rho_A = M_{\text{total}}/A_{\text{total}}$:

$$M_k = \rho_A A_k, \tag{6}$$

where A_k is the area of the clipped cell associated with sensor k. The resulting mass matrix is

$$\mathbf{M} = \text{diag}(M_1, \ldots, M_{N_p}), \tag{7}$$

where N_p defines the number of Voronoi partitions [7]. This method assigns a region of mass to each accelerometer based on proximity. This ensures that every point on the panel is mathematically associated with its nearest sensor, providing an objective basis for the lumped mass matrix.

Transformation to Modal Coordinates

Operational acceleration measurements $a_k(t)$ at N_p points are collected during road tests and assembled into the vector $\vec{a}(t)$. Modal accelerations are then obtained through projection onto the mode shapes:

$$\ddot{q}_n(t) = \vec{\psi}_n^T \mathbf{M} \vec{a}(t) = \sum_{k=1}^{N_p} (\vec{\psi}_n)_k M_k a_k(t). \tag{8}$$

Integration yields the modal velocities,

$$\dot{q}_n(t) = \int \ddot{q}_n(t)\, dt, \tag{9}$$

with appropriate high pass filtering to mitigate drift.

Computation of Dissipated Power

The transformation from physical to modal coordinates preserves the fundamental energy relationships of the system. In particular, the instantaneous power, defined as the inner product of velocity and force, is invariant under this transformation *provided that a sufficiently complete set of modes is retained to represent the motion*; with truncated modal bases, the invariance holds only for the projected component of the response. Thus, whether expressed in the physical coordinates of the measurement points or in the reduced modal coordinates, the computed power remains identical. This invariance ensures that the subsequent analysis of dissipated and transmitted power can be carried out entirely in the modal domain without loss of physical fidelity. The dissipated power per mode n is expressed as

$$P_n(t) = c_n [\dot{q}_n(t)]^2 = 2\zeta_n \omega_n [\dot{q}_n(t)]^2. \tag{10}$$

Summing across modes gives the total dissipated power,

$$P_{\text{dissipated}}(t) = \sum_{n=1}^{N_m} P_n(t). \tag{11}$$

The time-averaged dissipation over a duration T is

$$\overline{P}_{\text{dissipated}} = \sum_{n=1}^{N_m} 2\zeta_n \omega_n \langle [\dot{q}_n(t)]^2 \rangle, \tag{12}$$

where $\langle [\dot{q}_n(t)]^2 \rangle$ denotes the mean-square modal velocity. For the bounding analysis, a factor of $\beta = 3$ was assumed. The accumulated dissipated energy is obtained by integrating power over time,

$$E_{\text{dissipated}}(t) = \int_0^t P_{\text{dissipated}}(\tau)\, d\tau. \tag{13}$$

To bound the total vibrational energy exchange, we assume a boundary transmission factor β such that

$$P_{\text{transmitted}} = \beta\, P_{\text{dissipated}}. \tag{14}$$

Hence the bound on instantaneous power, average power, and cumulative energy are

$$P_{\text{bound}}(t) = (1+\beta)\, P_{\text{dissipated}}(t), \quad \overline{P}_{\text{bound}} = (1+\beta)\, \overline{P}_{\text{dissipated}}, \quad E_{\text{bound}}(t) = (1+\beta)\, E_{\text{dissipated}}(t), \tag{15}$$

with $\beta = 3$ in this work.

Coupling loss factors in structural assemblies are often comparable in magnitude to internal damping, and in cases of strong junctions or multiple coupling pathways the total loss factor can substantially exceed the internal component (Schiller, 2010) [8]. Studies in [9], and[10, 11] confirm that coupling loss factors vary widely with boundary conditions, motivating the back-of-the-envelope estimate of β adopted in this work. From the estimates in Table 2, the modal damping ratios fall in the range $\zeta \sim 0.006-0.033$, corresponding to internal loss factors of $\eta \approx 2\zeta, \sim 0.012-0.066$. Using $\sum \eta_{ij} \approx 0.06$ for a panel connected to two neighbors plus the ceiling and floor, the resulting $\beta = \frac{\sum \eta_{ij}}{\eta_i}$ spans ∼0.9–5 depending on the assumed internal loss factor.

The framework developed builds upon well-established practices in experimental modal analysis [5], including global curve fitting of frequency response functions [6] Alternative methods for estimating vibrational power flow include structural intensity approaches [12] and statistical energy analysis (SEA) [13], both of which require extensive spatial measurements or coupling loss factor data. In contrast, most energy harvesting research has focused on modeling specific transducers such as piezoelectric, electromagnetic, or triboelectric devices. By treating internal damping losses identified through EMA as an upper bound for harvestable energy, our method provides a harvester agnostic and operationally validated metric that can be applied consistently across different road environments.

Results and Discussion

Figure 7 show the modal velocity for the accelerometer S5, the total instantaneous power and the cumulative energy for the I-65 road segment. Note that the energy dissipated is cumulative with discontinuities at spikes in power. In order to quantify uncertainty in the mean dissipated power over I-65, the instantaneous power signal was aggregated into non-overlapping 30 s windows and the window-mean power was computed. The trip-average power was $\bar{P} = 1.565$ W per panel. A 95% confidence interval (CI) of $[1.448,\ 1.728]$ W was estimated in using a block bootstrap with 90 s contiguous windows (5000 resamples). The corresponding cumulative energy over the trip was $E_{\mathrm{trip}} \approx 4.11 \times 10^3$ J per panel.

Table 3 are estimations for a full 24-panel trailer wall, calculated by multiplying the results from the single instrumented panel by 24, assuming similar vibrational behavior across all panels. The vibration energy data collected across 19 distinct road segments reveals substantial variation in both energy harvesting potential and power intensity, highlighting key opportunities and limitations for vibration-based energy systems. The interstate corridor I-65 stands out, generating the highest cumulative energy output (over 54.6 kJ) and extreme peak power levels (over 27.5 kW for 24 panels), making it the most promising candidate for high-yield energy harvesting. Other major corridors such as US52/31, US421, and SR26 also demonstrate considerable energy accumulation (ranging from approximately 6.5 to 10.3 kJ), suggesting that heavily trafficked, long-duration road segments are particularly well-suited for sustained energy recovery or self-powered infrastructure applications.

Table 3 Summary of Vibration-Based Power and Energy Estimates Across Road Segments (24 Panels). "+Bound" indicates inclusion of boundary transmission with $\beta = 3$, i.e., values are $(1 + \beta) = 4$ times the dissipated estimates

Road	Time (s)	Mean Power (W)	Peak Power (W)	Energy (J)	Mean+Bound (W)	Peak+Bound (W)	Energy+Bound (J)
Russell	182.12	0.568	5.13	103.51	2.273	20.54	414.04
Williams	93.99	5.231	18.93	491.69	20.93	75.70	1,966.76
Harrison	100.03	3.105	27.86	310.55	12.42	111.43	1,242.20
Tapawingo	101.99	0.548	3.29	55.92	2.193	13.17	223.67
South	583.96	11.42	51.19	6,668.72	45.68	204.77	26,674.89
US52/31	762.81	13.54	47.74	10,328.34	54.16	190.95	41,313.36
US52	98.98	9.20	1,874.90	910.47	36.80	7,499.60	3,641.88
SR28E	696.61	0.828	148.80	576.84	3.312	595.19	2,307.38
SR28	226.95	24.27	99.65	5,508.30	97.08	398.62	22,033.21
I65	2,626.54	20.81	6892.19	54,649.04	83.23	27,568.77	218,596.18
SR38	56.05	1.766	156.00	98.98	7.064	623.99	395.91
SMeridian	135.01	0.668	13.67	90.22	2.673	54.70	360.89
SR18	408.00	1.797	102.15	733.08	7.187	408.60	2,932.31
SR26	1,423.94	6.474	173.44	9,218.06	25.89	693.76	36,872.25
SR27	722.00	6.070	1,731.68	4,382.63	24.28	6,926.71	17,530.53
SR43	156.02	1.932	26.26	301.40	7.727	105.03	1,205.61
US24	1,852.94	2.999	1,122.63	5,556.12	11.99	4,490.52	22,224.47
US421	1,473.88	4.435	2,067.20	6,536.37	17.74	8,268.79	26,145.48
WHarrison	127.98	1.237	15.23	158.36	4.949	60.91	633.43

In contrast, several roads including SR38, Tapawingo and West Harrison produced minimal energy yields (below 150 J total), primarily due to short durations and lower vibrational intensity. These segments are unlikely to support active energy harvesting and may instead serve as control or baseline environments for vibration analysis. Notably, many roads exhibit

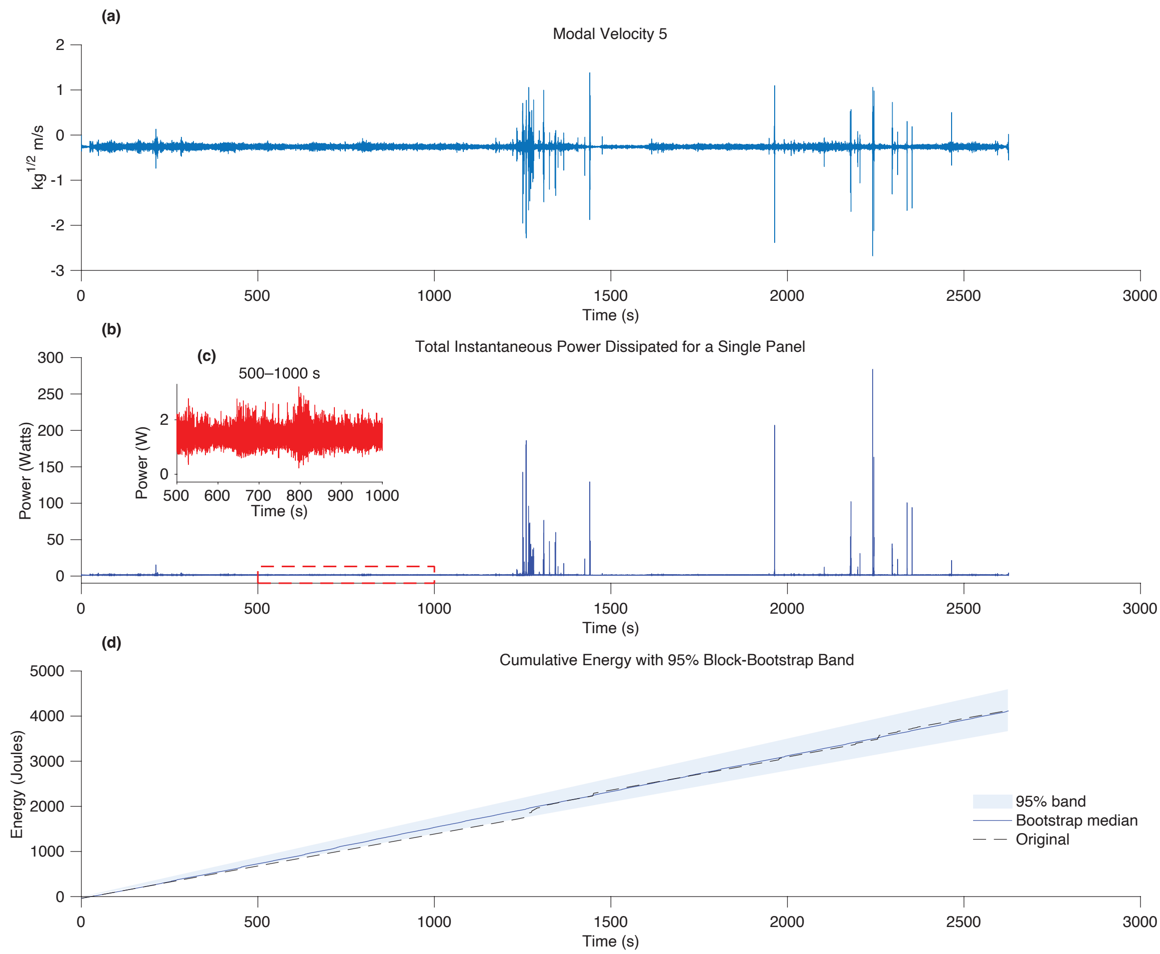

Fig. 7 Experimental energy in first rear panel for I-65: (a) modal velocity of mass 5, (b) instantaneous power, and (c) accumulated energy with 95% Block-Bootstrap band. The modal velocity has units of $kg^{1/2}$m/s, which is characteristic of modal coordinates derived from mass-normalized mode shapes where the modal mass is unity. Inset in (b) shows the power from 500 to 1000 s interval (red box in the main trace) on I-65. Note that energy increases monotonically with time, while the instantaneous power exhibits intermittent bursts tied to transient excitations

significant increases in RMS and peak power when boundary effects are included in the analysis. For instance, RMS power often increased by a factor of three to four when boundaries were modeled, indicating that edge effects or mechanical constraints on panel configurations play a nontrivial role in strain amplification and energy transduction.

Several roads, including US52, SR28E, and SR38, exhibit unusually high peak powers relative to their overall energy output, implying short-duration, high-intensity excitations such as bridge joints, pavement gaps, or surface anomalies. These conditions may be ideal for triggering threshold-based systems (e.g., damage detection or alert beacons) rather than continuous energy harvesting. Overall, the data indicate that deployment strategies should be differentiated based on road characteristics: highways and arterials with sustained vibrations are optimal for energy recovery, while urban and low-yield roads may benefit more from passive sensing systems or localized energy storage. The clear performance disparities across road types underscore the importance of site-specific design in energy harvesting applications.

Limitations

This work has several important limitations. First, modal truncation excludes the dissipative contributions of higher modes, so the present estimates should be regarded as a *conservative lower bounds* unless the retained modes capture a sufficiently large fraction of the total effective modal mass. Second, not all modes were reliably excited across the different impact configurations; only those consistently identified in every modal test were retained. This restriction improves robustness but further reduces modal coverage and may bias the dissipation estimates downward by omitting intermittently excited modes. Another source of uncertainty is in the mass discretization; the lumped mass matrix is derived from a nonuniform Voronoi partition around the sensors. While a uniform partition is not feasible without repeating the experiment, increasing the number and uniformity of masses would systematically improve the quadrature accuracy of the modal projections and reduce discretization bias. Finally, this study assumes that the single panel tested is representative of the other trailer panels. In practice, the selected edge panel may deform differently than middle panels or opposite-side edge panels due to boundary conditions and asymmetric load paths. As such, the extrapolation of results to the full trailer should be viewed cautiously until validated by measurements on additional panel locations.

Conclusion

This study presented an integrated framework to quantify vibrational power dissipation in semi-trailer panels by combining experimental modal analysis with operational road testing. Using modal impact tests, the panel's natural frequencies, damping ratios, and mode shapes were identified and formed the basis of a reduced-order modal model. Operational accelerometer data collected across 19 road segments were then projected into modal coordinates, enabling estimation of modal velocities and subsequent calculation of dissipated vibrational power.

The results demonstrate that vibrational energy dissipation in trailer panels is dominated by broadband responses in the 2–20 Hz frequency range, rather than by isolated resonances. Among the tested conditions, interstate highway segments such as I-65 exhibited the highest energy accumulation (exceeding 54 kJ for 24 panels) and peak power levels (over 27 kW), while local or short road segments such as West Harrison and Russell produced negligible energy yields. These findings highlight the strong dependence of energy availability on road type and driving conditions, suggesting that deployment of energy harvesting devices should be tailored to specific operational environments.

Although this analysis focuses on a single panel, boundary effects and mass loading from neighboring panels were implicitly captured in the measured modal parameters, providing a lower bound estimate of energy dissipation. Nonetheless, additional work is required to explicitly quantify transmitted power across panel boundaries and to assess the collective response of the full trailer assembly.

Future research should extend this framework to multi-panel models, investigate fatigue and durability effects, and integrate prototype energy harvesting devices (piezoelectric, triboelectric, or electromagnetic) to validate practical performance. By establishing a physically consistent method for estimating vibrational energy dissipation, this work provides a foundation for designing next-generation trailer panels capable of harvesting ambient vibrations to reduce alternator load and improve the energy efficiency of heavy vehicles.

Acknowledgments The authors gratefully acknowledge the support of Wabash for providing access to the trailer panels used in this study and for funding this study. We extend special thanks to Andrzej Wylezinski and Michael Bodey for their guidance, technical input, and continued support throughout this work. Their collaboration and insights were essential to the successful execution of the research. We also thank Cody Bahler and Jose Romero for their assistance in operating the semi-truck during testing.

Appendix: Derivation of Power Quantification

The equations of motion of a trailer panel can be written in physical coordinates as

$$\mathbf{M}\,\ddot{\vec{x}}(t) + \mathbf{C}\,\dot{\vec{x}}(t) + \mathbf{K}\,\vec{x}(t) = \vec{f}(t), \tag{16}$$

where $\vec{x}(t)$ are nodal displacements, $\vec{f}(t)$ are applied forces, and $\mathbf{M}, \mathbf{C}, \mathbf{K}$ are the mass, damping, and stiffness matrices. The damping matrix is assumed to be proportional to $\mathbf{M}$ and $\mathbf{K}$.

Let $\boldsymbol{\Phi} = [\,\vec{\psi}_1 \ \cdots \ \vec{\psi}_{N_m}\,]$ denote the retained set of mass-normalized mode shapes identified from experimental modal analysis (EMA). The displacement and velocity fields are expressed as

$$\vec{x}(t) = \boldsymbol{\Phi}\,\vec{q}(t), \qquad \dot{\vec{x}}(t) = \boldsymbol{\Phi}\,\dot{\vec{q}}(t), \tag{17}$$

where $\vec{q}(t)$ are modal coordinates.

Substituting into the governing equations and premultiplying by $\mathbf{\Phi}^\mathsf{T}$ gives the decoupled modal equations of motion:

$$\ddot{q}_n(t) + 2\zeta_n\omega_n\dot{q}_n(t) + \omega_n^2 q_n(t) = g_n(t), \qquad n = 1, \ldots, N_m, \tag{18}$$

where ω_n and ζ_n are the natural frequency and damping ratio from EMA, and $g_n(t) = \vec{\psi}_n^\mathsf{T} \vec{f}(t)$ are modal forces.

In this case, the applied force vector is replaced by the equivalent damping forces, $\mathbf{C}\dot{\vec{x}}(t)$, so that the power expression reduces to the rate of energy dissipated through damping. This substitution leads directly to the modal form of the dissipated power, expressed as a sum over the modal damping contributions. The instantaneous mechanical power is preserved under this transformation:

$$P(t) = \dot{\vec{x}}^\mathsf{T} \vec{f}(t) = \dot{\vec{q}}^\mathsf{T} \vec{g}(t), \tag{19}$$

and using the damping forces $\vec{f}(t) = \mathbf{C}\,\dot{\vec{x}}(t) = \mathbf{C\Phi}\dot{\vec{q}}(t)$, the dissipated power is

$$P_{\text{diss}}(t) = \dot{\vec{q}}^\mathsf{T} \mathbf{C}_m \dot{\vec{q}} = \sum_{n=1}^{N_m} c_n\, \dot{q}_n^2(t), \tag{20}$$

where $\mathbf{C}_m = \mathbf{\Phi}^T \mathbf{C} \mathbf{\Phi}$ and the cumulative dissipated energy over $[0, T]$ is

$$E_{\text{diss}}(T) = \int_0^T P_{\text{diss}}(t)\, dt. \tag{21}$$

In practice, operational accelerations $\vec{a}(t) = \ddot{\vec{x}}(t)$ are recorded during road testing, and the mass matrix $\mathbf{M}$ is approximated by lumped weights $\{M_k\}$ assigned via sensor-based partitioning. Modal accelerations are obtained from

$$\ddot{\vec{q}}(t) = \mathbf{\Phi}^\mathsf{T} \mathbf{M}\, \ddot{\vec{x}}(t), \tag{22}$$

and integrated to yield $\dot{\vec{q}}(t)$, which are then used to compute $P_{\text{diss}}(t)$ and $E_{\text{diss}}(T)$.

References

1. Ropovik, R., Hatala, M., and Dobransky, J. "Optimization of lighting for truck with lifting platform". *Manufacturing Technology*, 24(Special Issue):TEAM2024–00031 (2024)ifnextchar.gobble.
2. Arrieta, A.F., Wagg, D.J., and Neild, S.A. "A piezoelectric bistable plate for nonlinear broadband energy harvesting". *Applied Physics Letters*, 97(10):104102 (2010)ifnextchar.gobble.
3. Erturk, A. and Inman, D.J. *Piezoelectric Energy Harvesting*. John Wiley & Sons (2011)ifnextchar.gobble.
4. Tao, H. and Gibert, J. "Multifunctional mechanical metamaterials with embedded triboelectric nanogenerators". *Advanced Functional Materials*, 30(23):2001720 (2020)ifnextchar.gobble.
5. Ewins, D.J. *Modal Testing: Theory, Practice and Application*. Research Studies Press, 2nd edition (2000)ifnextchar.gobble.
6. Richardson, M.H. and Formenti, D.L. "Global curve fitting of frequency response measurements using the rational fraction polynomial method". In *Proceedings of the 3rd International Modal Analysis Conference (IMAC)*, pages 390–397, Orlando, Florida (1985)ifnextchar.gobble. Structural Measurement Systems, San Jose, California.
7. O'Rourke, J. *Computational Geometry in C*. Cambridge University Press (1998)ifnextchar.gobble.
8. Schiller, N.H. "Impact of damping uncertainty on sea model response". Technical Report NASA/TM–2010-216352, NASA Langley Research Center (2010)ifnextchar.gobble. Accessed: 2025-09-21.
9. Langley, R.S. "A derivation of the coupling loss factors used in statistical energy analysis". *Journal of Sound and Vibration*, 141(2):207–219 (1990)ifnextchar.gobble.
10. Park, W.S. and Kim, Y.H. "Variability of the coupling loss factor between two subsystems". *Journal of Sound and Vibration*, 279(1-2):357–371 (2005)ifnextchar.gobble.
11. Su, J. and Zheng, L. "An identification method for the effective coupling loss factor based on the hybrid fe–sea model". *Applied Sciences*, 13(6):3687 (2023)ifnextchar.gobble.
12. Booth, W. and Hammond, J.P. "Structural intensity and power flow techniques in vibration". *Journal of Sound and Vibration*, 150(3):319–335 (1991)ifnextchar.gobble.
13. Lyon, R.H. and DeJong, R.G. *Theory and Application of Statistical Energy Analysis*. Butterworth-Heinemann, 2nd edition (1995)ifnextchar.gobble.